ᴓ OPEN ACCESS

Thermal and Viscous Irreversibilities Analysis in a Liquid Metal Phase Change Counter Flow Heat Exchanger

Élcio Nogueira[1*], Diniz Felix dos Santos Filho[1,2]

[1]Centro Universitário Dom Bosco – UniDomBosco
[2]Centro Universitário UNIFOA

*Corresponding author: Élcio Nogueira
Centro Universitário Dom Bosco – UniDomBosco

Abstract	Original Research Article

Sodium, a liquid metal, is utilized in a heat exchanger system coupled to a nuclear reactor to produce hydrogen. The subcooled liquid metal enters a counterflow heat exchanger, undergoes a phase change, and exits as superheated vapor. The sodium heating process occurs through heat exchange with superheated helium vapor in three phases: subcooled liquid, saturated vapor, and superheated vapor. This article analyzes the thermal and hydraulic performance of the three stages of the heat exchanger through thermal and viscous irreversibilities using analytical simulation. The solution obtained is based on applying the thermal efficiency method and the second law of thermodynamics. The thermodynamic Bejan number, the relationship between thermal irreversibility and total irreversibility, allows a cost-benefit analysis when determining thermal performance and viscous dissipation. The essential physical quantities used in the analysis are the lengths and internal diameters of the three segments of the heat exchanger. The results are analyzed and compared with previous analytical work published in the literature. Numerical and graphical results are obtained for temperature profiles, thermal effectiveness, heat transfer rate, thermal irreversibilities, pressure drops, viscous irreversibilities, entropy generation rate, and Bejan numbers. It is demonstrated that the cost-benefit is highly advantageous when the diameter used for the internal tubes of the three segments is equal to the diameter of the saturated sodium vapor section, corresponding to ¼ of the speed of sound in the tube.
Keywords: Thermal irreversibility; Viscous irreversibility; Liquid metal phase change; Counter flow heat exchanger.

1. INTRODUCTION

The article's main objective is to analyze a counterflow heat exchanger's thermal and hydraulic performance where one of the fluids is sodium and the other is helium. Sodium exchanges heat with superheated helium in three distinct phases. Sodium enters the heat exchanger as a subcooled liquid and leaves it as superheated vapor, passing through the transition as saturated vapor. The inlet temperature of sodium equals 120 ℃, and that of helium vapor is 1027 ℃. The theoretical simulation uses the thermal efficiency method to determine thermal and viscous irreversibilities. The parameter used for the cost-benefit analysis of the heat exchanger is the Bejan thermodynamic number, which represents the relationship between thermal irreversibility and total irreversibility, the thermal irreversibility added to the viscous irreversibility. The most relevant variables in the analysis are the tubes' diameters in each section of the heat exchanger and their respective lengths. Teams of researchers exhaustively studied the system, and many aspects related to the

fluids, the materials used, and the ideal configuration of the heat exchanger were considered. However, none of the theoretical work used the methodology presented here.

Piyush Sabharwall *et al.,* [1] analyze a heat exchanger to transfer energy from a nuclear power plant to a hydrogen production plant. To optimize heat transfer, they use liquid metal in a phase change process since heat exchangers that use this method are more efficient, mainly due to the latent heat of vaporization. They use superheated helium vapor as the primary element and subcooled liquid sodium as the secondary element in heat exchange. They introduce the general pressure drop in the heat exchanger into the analysis and clarify that the study can guide experimental work related to nuclear plants.

Piyush Sabharwall, Eung Soo Kim, and Nolan Anderson [2] mention that selecting a specific type of heat exchanger involves many variables, which depend

mainly on its application. They state that the main criterion to be analyzed is the thermo-hydraulic performance, which requires effectiveness in heat exchange and minimum fouling, that is, the search for a higher global heat transfer coefficient and lower pumping power. They clarify that better thermal performance and lower thermal and frictional resistance result in greater thermodynamic and economic efficiency, as they meet the highest performance requirements with minimum life cycle costs.

Piyush Sabharwall and Eung Soo Kim [3] state that heat exchangers that work at high temperatures have applications in many industrial sectors, including nuclear power plants, and that these heat exchangers must use larger diameters to minimize the pressure drop. They state that liquid metals are used at high temperatures instead of steam, as these work at high pressure and require high-thickness tubes. They clarify that the heat exchanger that operates at high temperatures must offer reliability and long functional life since the materials used in its construction are expensive, with costs increasing from 675 ºC. They describe a thermosiphon system and highlight the benefit of using it in a hydrogen production plant. They emphasize that the emphasis on energy conservation stipulates using heat pipes and thermosyphons in a heat recovery system. Still, it should be noted that thermosyphons have lower thermal resistance and operational limits that are more suitable for high temperatures, in addition to lower manufacturing costs.

Piyush Sabharwall [4] reports that developing high-temperature reactors for hydrogen production is a high priority. One option is to use two-phase heat transfer in a high temperature thermosyphon. In this type of reactor, heat transport occurs through evaporation and condensation, taking advantage of gravitational force and being able to transfer high rates of heat over appreciable distances in a practically isothermal way without the need for external pumping. He clarifies, however, that transporting fluids at high temperatures involves significant challenges and that single-phase helium under low pressure is an option but should not be dedicated exclusively to hydrogen production. He concludes that the research allows decision-making regarding the thermosyphon coupled between the nuclear reactor and the hydrogen production plant.

Anna M. Wagner [5] reports that thermosiphons have numerous technological applications, including in the nuclear industry. She presents an article discussing the applications of thermosyphons in cold regions. Reports that thermosyphons were initially designed as passive tubes but were changed to act as active and hybrid systems. The thermosyphon is described as a tube that uses a working fluid to transport thermal energy and operates by vaporization at one end and condensation at the other. After condensation, the working fluid returns to the evaporation region through gravity. It states that

the heat transfer rate in a thermosyphon depends on the working fluid, the system's symmetry, the construction material, and the external environment that exchanges heat and that high-density, low-viscosity fluids contribute to the return to the evaporator.

Bala Abdullahi, Raya K. Al-dadah, and Sa'ad Mahmoud [6] argue that heat pipes are vital in many engineering systems as they enable high performance in heat transfer between fluids and investigate heat pipes under different operating conditions. In the work developed, they present an overview of heat pipes and focus mainly on aspects related to thermosyphons, discussing numerical and experimental approaches that enable better performance. They discuss details of practical work, modeling, and simulations on thermosyphons, including information related to filling rate, working fluid, and inclination angles, among others. Finally, they present details related to research that describes factors that affect thermosyphon operation and where they apply in engineering systems.

Shanbin Shi *et al.,* [7] report that fission energy removal is achieved by high-temperature heat pipes in nuclear microreactors and that modeling the two-phase flow internal to the heat pipe is vital for such systems. They present a study of two-phase heat flow applicable to heat pipes under normal and transient operating conditions, including mass, momentum, and energy conservation equations for the liquid film, vapor, and drops. The developed model includes interfacial constitutive equations for heat and mass transfer to film and droplets, with the introduction of valid correlations for annular film thickness. They believe that the study presented will serve as a basis for research activities in microreactors cooled by heat pipes and that it is essential to include experiments that use fluids at high temperatures in future studies. In this sense, they provide instructions for new test installations using liquid metal as working fluid and add that new models can be implemented using modern computational tools.

Andrijana D. Stojanović *et al.,* [8] present a review of analytical and numerical works related to heat transfer in nucleated boiling. They clarify that understanding the nucleated boiling process is vitally important due to safety issues in nuclear centers, fusion reactors, and other industrial processes. They state that many studies are related to nucleated boiling, but the current understanding of this phenomenon is incipient concerning the various sub-processes and their interactions. Most of the existing work seeks to find methods that make it possible to increase heat exchange, but they do not clarify the phenomenon of boiling itself despite helping to understand the nucleation process of vapor bubbles. Despite the great advances in numerical models, the boiling process is difficult to predict due to the complex phenomena involved. They conclude that there is a need for new experimental research and measurement techniques to be considered and that new

models must be free of empirical parameters; that is, they must be dependent on a reduced number of adjustable parameters.

Dawid Taler [9] analyzes the heat transfer process in a turbulent liquid metal regime in a circular duct with a prescribed heat flow at the surface. New heat transfer correlations are developed using the universal velocity profile experimentally determined by Reichardt and use different relationships for the turbulent Prandtl number. He considers four models for turbulent Prandtl numbers and concludes that all correlations developed for Nusselt number approach experimental data satisfactorily.

Élcio Nogueira [10] revisits the concepts of thermal efficiency, thermal and viscous irreversibilities, the second law of thermodynamics, and Bejan's thermodynamic number and applies them to a problem related to thermal exchange between two fluids. It solves the problem of parallel and counterflow flows using dimensional analysis. He highlights that the thermal efficiency method is valuable for analyzing, sizing, and optimizing heat exchangers.

Élcio Nogueira [11] applies the thermal efficiency method to determine the thermal performance of a heat pipe heat exchanger with individual fins used in an air conditioning system. The solutions for the evaporator and condenser are presented individually, associated with the global theoretical performance of the

heat exchanger, and compared with global experimental results from the literature. Mainly determines the thermal and viscous irreversibilities and the thermodynamic Bejan number for the cost-benefit analysis of the heat exchanger. He demonstrated that the theoretical-experimental comparison is consistent and that the method can be used as a design and analysis tool for heat exchangers.

2. METHODOLOGY

The counterflow heat exchanger consists of concentric tubes with helium vapor flowing in the annular region and liquid sodium metal in the inner tube. Subcooled sodium enters at one end of the heat exchanger and helium vapor at the other. The sodium saturation temperature, equal to 833 ºC, is a reference for simulating flow and heat transfer in the three regions of the heat exchanger. The outer diameter is uniform, and the inner diameter varies during the simulation. Thermal resistances related to tube surfaces are neglected compared to the thermal resistances associated with flow regimes. The properties of the fluids are obtained approximately considering the temperature variation range under analysis in each region.

Figure 1 represents the heat exchange process between superheated helium vapor and the three regions associated with sodium: region 1 - subcooled liquid, region 2 - saturated vapor, and region 3 - superheated vapor.
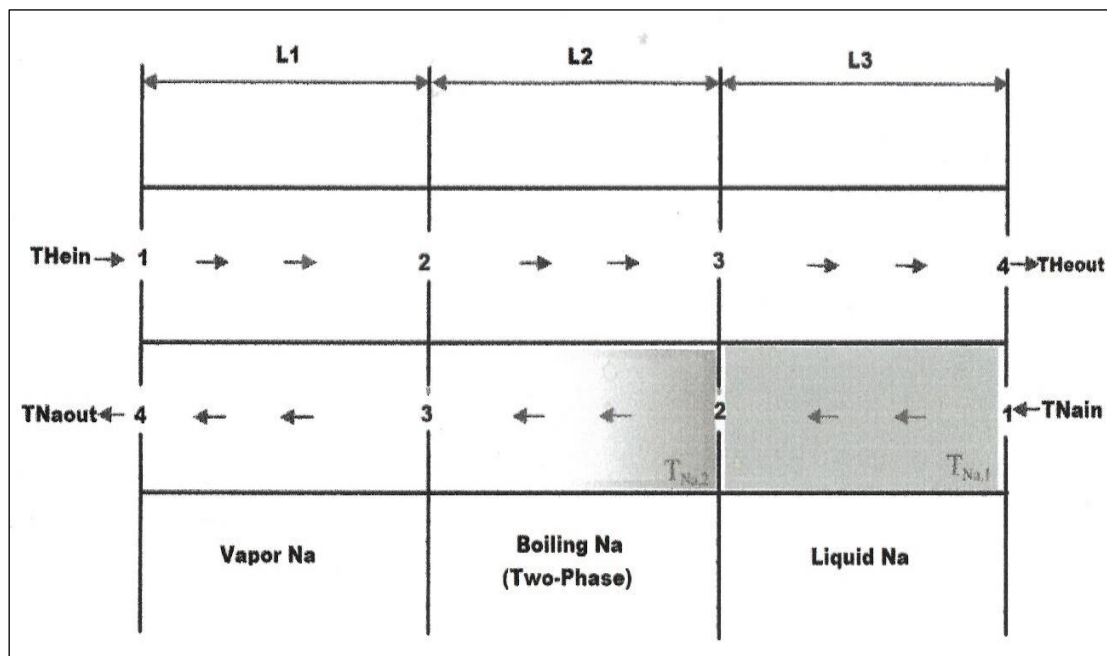
Figure 1 – Liquid Metal Phase Heat Exchanger - LMPCHE (Adapted by Piyush Sabharwall *et al.,* [1])

2.1 Thermal solution

The properties associated with Helium depend on the vapor mixing temperature in the region under analysis. The Helium mixing temperature in the region under analysis is represented by THe_i, where the index

varies from 1 to 3. Petersen, H. [12], Vincent D. Arp, and Robert D. McCarty [13] provide tables properties of Helium [Equation (1) to Equation (7)].

$$\rho_{Hei} = 0.1717547693d0 - 0.0005024738072 * THe_i + 9.528424492d - 7 * THe_i ** 2.d0$$
$$-1.020764019d - 9 * THe_i ** 3.d0 + 5.538255567d - 13 * THe_i ** 4.d0 \tag{1}$$
$$- 1.177254392d - 16 * THe_i ** 5.d0 \quad 1 \leq i \leq 3$$

$$k_{Hei} = 0.148407961d0 + 0.0003254147293d0 * THe_i - 4.305657603d - 8 * THe_i ** 2.d0 \tag{2}$$

$$\mu_{Hei} = (1.929583717d0 + 0.004096498682 * THe_i - 5.313746426d - 7 * THe_i ** 2.d0) * 1.d - 5 \tag{3}$$

$$Pr_{Hei} = 0.6725624682d0 - 2.199176297d - 5 * THe_i + 2.590560079d - 8 * THe_i ** 2.d0$$
$$-2.328029436d - 11 * THe_i ** 3.d0 \tag{4}$$
$$+1.17454495d - 14 * THe_i ** 4.d0 - 2.431817654d - 18 * THe_i ** 5.d0$$

$$v_{Hei} = \frac{\mu_{Hei}}{\rho_{Hei}} \tag{5}$$

$$\alpha_{Hei} = \frac{\mu_{Hei}}{Pr_{Hei}} \tag{6}$$

$$Cp_{Hei} = \frac{v_{Hei}}{\alpha_{Hei}} \tag{7}$$

ρ_{Hei} is the density of helium vapor. k_{Hei} is the thermal conductivity of helium vapor in region i. μ_{Hei} is the dynamic viscosity of helium vapor. v_{Hei} is the dynamic viscosity associated with helium vapor. α_{Hei} is the thermal diffusivity of helium vapor in region i. The specific heat of helium vapor in region i is represented by Cp_{Hei}. Pr_{Hei} is the Prandtl number of Helium in region i.

The properties of Sodium in the two-phase flow region are associated with the properties of saturated liquid, related to the index l, and saturated vapor, related to the index v. The tables properties of Sodium are provided by Joanne K. Fink and Leonard Leibowitz [14] and by G. H. Golden and J. V. Tokar [15] [Equation (8) to Equation (19)].

$$\rho_{Nal} = -0.2382637363d0 * TNa_2 + 951.134744d0 \tag{8}$$

$$\rho_{Nav} = (-1942.324038d0 + 9.805341382d0 * TNa_2 - 0.01643668511d0 * TNa_2 ** 2.d0$$
$$+9.251732712d - 6 * TNa_2 ** 3.d0) * 1.d3 \tag{9}$$

$$k_{Nal} = 91.21074266d0 - 0.04824000559d0 * TNa_2 + 6.873126873d - 7 * TNa_2 ** 2.d0 \tag{10}$$

$$k_{Nav} = -0.00578082968d0 + 6.85950024d - 5 * TNa_2 + 6.578942795d - 8 * TNa_2 ** 2.d0$$
$$-1.208200401d - 10 * TNa_2 ** 3.d0 + 4.632867133d - 14 * TNa_2 ** 4.d0 \tag{11}$$

$$\mu_{Nal} = (7.549325321d0 - 0.02161616967d0 * TNa_2 + 3.465090376d - 5 * TNa_2 ** 2.d0$$
$$-3.030746977d - 8 * TNa_2 ** 3.d0 + 1.361249488d - 11 * TNa_2 ** 4.d0$$
$$-2.453808446d - 15 * TNa_2 ** 5.d0) * 1.d - 4 \tag{12}$$

$$\mu_{Nav} = (933.0641319d0 + 1.555217815 * TNa_2 + 0.0003932320867d0 * TNa_2 ** 2.d0$$
$$-1.716200466d - 7 * TNa_2 ** 3.d0) * 1.d - 8 \tag{13}$$

$$Cp_{Nal} = 2.022230309d0 - 0.005312730163d0 * TNa_2 + 1.501227267d - 5 * TNa_2 ** 2.d0$$
$$-2.13879551d - 8 * TNa_2 ** 3.d0 + 1.514270833d - 11 * TNa_2 ** 4.d0 \tag{14}$$
$$-4.166666667d - 15 * TNa_2 ** 5.d0$$

$$Cp_{Nav} = (0.1013238839d0 + 0.002248844802d0 * TNa_2 + 2.089437138d - 5 * TNa_2 ** 2.d0$$
$$-4.723338971d - 8 * TNa_2 ** 3.d0 + 3.569885839d - 11 * TNa_2 ** 4.d0 \tag{15}$$
$$-9.307692308d - 15 * TNa_2 ** 5.d0) * 1.d2$$

$$v_{Nal} = \frac{\mu_{Nal}}{\rho_{Nal}} \tag{16}$$

$$v_{Nav} = \frac{\mu_{Nav}}{\rho_{Nav}} \tag{17}$$

$$Pr_{Nal} = \frac{v_{Nal}}{\alpha_{Nal}} \tag{18}$$

$$Pr_{Nav} = \frac{v_{Nav}}{\alpha_{Nav}} \tag{19}$$

ρ_{Na} is the density of Sodium, the thermal conductivity is represented by k_{Na}, the dynamic viscosity by μ_{Na}, the specific heat by Cp_{Na}, the kinematic viscosity by v_{Na}, and the Prandtl number by Pr_{Na}. The thermal diffusivity is given by $\alpha_{Na} = \frac{k_{Na}}{\rho_{Na}Cp_{Na}}$.

$$T_{sat} = 833.0 \text{ ºC } fixed \tag{20}$$

T_{sat} is the saturation temperature of Sodium.

$$THe_{in1} = 1027 \text{ ºC } fixed \tag{21}$$

THe_{in1} is the inlet temperature of the helium vapor in the heat exchanger.

$$TNa_{in3} = 120 \text{ ºC } fixed \tag{22}$$

TNa_{in3} is the temperature at which Sodium enters the heat exchanger.

$$TNa_2 = T_{sat} \ fixed \tag{23}$$

$$\dot{m}_{He} = 81.59 \frac{kg}{s} \ fixed \tag{24}$$

$$D_{He} = 1.551 \ m \tag{25}$$

The mass flow rate of Helium is 81.59 kg/s, and the external diameter is 1.551 m.

$$\dot{m}_{Na} = 9.794 \frac{kg}{s} \ fixed \tag{26}$$

$$D_{Na1} = 0.122 \ m \ default \tag{27}$$

$$D_{Na3} = 0.122 \ m \ default \tag{28}$$

The mass flow rate of Sodium equals 9.794 kg/s, and the internal diameter in regions 1 and 3 equals 0.122 m by default. The energy per unit of mass exchanged between the fluids during two-phase flow in Region 2 is given by:

$$h_{Nalv} = (4771.697082d0 - 1.000857055d0 * TNa_2 - 0.0001022855894d0 * TNa_2 ** 2.d0 \\ + 9.906759907d - 8 * TNa_2 ** 3.d0) * 1.d3 \tag{29}$$

The properties of Sodium in Regions 1 and 3 are obtained by Equation (30) to Equation (41) :

$$\rho_{Na1} = -0.2382637363d0 * TNa_1 + 951.134744d0 \tag{30}$$

$$k_{Na1} = 91.21074266d0 - 0.04824000559d0 * TNa_1 + 6.873126873d - 7 * TNa_1 ** 2.d0 \tag{31}$$

$$\mu_{Na1} = (7.549325321d0 - 0.02161616967d0 * TNa_1 + 3.465090376d - 5 * TNa_1 ** 2.d0 \\ - 3.030746977d - 8 * TNa_1 ** 3.d0 + 1.361249488d - 11 * TNa_1 ** 4.d0 \\ - 2.453808446d - 15 * TNa_1 ** 5.d0) * 1.d - 4 \tag{32}$$

$$Cp_{Na1} = 2.022230309d0 - 0.005312730163d0 * TNa_1 + 1.501227267d - 5 * TNa_1 ** 2.d0 \\ - 2.13879551d - 8 * TNa_1 ** 3.d0 + 1.514270833d - 11 * TNa_1 ** 4.d0 \\ - 4.166666667d - 15 * TNa_1 ** 5.d0 \tag{33}$$

$$v_{Na1} = \frac{\mu_{Na1}}{\rho_{Na1}} \tag{34}$$

$$Pr_{Na1} = \frac{v_{Na1}}{\alpha_{Na1}} \tag{35}$$

$$\rho_{Na3} = (-1942.324038d0 + 9.805341382d0 * TNa_3 - 0.01643668511d0 * TNa_3 ** 2.d0 \\ + 9.251732712d - 6 * TNa_3 ** 3.d0) * 1.d3 \tag{36}$$

$$k_{Na3} = -0.00578082968d0 + 6.85950024d - 5 * TNa_3 + 6.578942795d - 8 * TNa_3 ** 2.d0 \\ - 1.208200401d - 10 * TNa_3 ** 3.d0 + 4.632867133d - 14 * TNa_3 ** 4.d0 \tag{37}$$

$$\mu_{Na3} = (933.0641319d0 + 1.555217815 * TNa_3 + 0.0003932320867d0 * TNa_3 ** 2.d0 \\ - 1.716200466d - 7 * TNa_3 ** 3.d0) * 1.d - 8 \tag{38}$$

$$Cp_{Na3} = (0.1013238839d0 + 0.002248844802d0 * TNa_3 + 2.089437138d - 5 * TNa_3 ** 2.d0 \\ - 4.723338971d - 8 * TNa_3 ** 3.d0 + 3.569885839d - 11 * TNa_3 ** 4.d0 \\ - 9.307692308d - 15 * TNa_3 ** 5.d0) * 1.d2 \tag{39}$$

$$v_{Na3} = \frac{\mu_{Na3}}{\rho_{Na3}} \tag{40}$$

$$Pr_{Na3} = \frac{v_{Na3}}{\alpha_{Na3}} \tag{41}$$

The temperatures $TNa_1 \ and \ TNa_3$ are mixing temperatures in the regions under analysis.

$$A_{Hei} = \frac{\pi(D_{He}^2 - D_{Nai}^2)}{4} \quad 1 \le i \le 3 \tag{42}$$

A_{Hei} is the helium flow area.

$$Per_{Hei} = \pi(D_{He} + D_{Nai}) \quad 1 \le i \le 3 \tag{43}$$

$$Dh_{Hei} = \frac{4A_{Hei}}{Per_{Hei}} \quad 1 \le i \le 3 \tag{44}$$

Dh_{Hei} is the hydraulic diameter associated with Helium.

$$Re_{Hei} = \frac{\dot{m}_{He} Dh_{Hei}}{A_{Hei} \mu_{Hei}} \quad 1 \le 1 \le 3 \tag{45}$$

$$V_{Hei} = \frac{\dot{m}_{He}}{\rho_{Hei} A_{Hei}} \quad 1 \le i \le 3 \tag{46}$$

Re_{Hei} is the Reynolds number associated with Helium, and the velocity is represented by V_{Hei} .

$$Nu_{Hei} = 0.022 Re_{Hei}^{0.8} Pr_{Hei}^{0.5} \quad 1 \le i \le 3 \tag{47}$$

Nu_{Hei} is the Nusselt number associated with helium vapor given by W. M. Kays and M. E. Crawford[16].

$$h_{Hei} = \frac{Nu_{Hei} k_{Hei}}{Dh_{Hei}} \quad 1 \le i \le 3 \tag{48}$$

The convection heat transfer coefficient is represented by h_{Hei} .

$$A_{Nai} = \frac{\pi D_{Nai}^2}{4} \quad 1 \le i \le 3 \tag{49}$$

The sodium flow area is represented by A_{Nai} .

$$Per_{Nai} = \pi D_{Nai}^2 \quad 1 \leq i \leq 3 \tag{50}$$

$$Dh_{Nai} = \frac{4A_{Nai}}{Per_{Nai}} \quad 1 \leq i \leq 3 \tag{51}$$

Dh_{Nai} is the hydraulic diameter associated with Sodium.

$$Re_{Nai} = \frac{\dot{m}_{Nai}Dh_{Nai}}{A_{Nai}\mu_{Nai}} \quad 1 \leq i \leq 3 \tag{52}$$

$$V_{Nai} = \frac{\dot{m}_{Nai}}{\rho_{Nai}A_{Nai}} \quad 1 \leq i \leq 3 \tag{53}$$

The Reynolds number associated with Sodium is represented by Re_{Nai} , and V_{Nai} is the velocity.

$$Nu_{Nai} = 6.3 + Re_{Nai}^{0.85}Pr_{Nai}^{0.93} \quad i = 1 \; or \; i = 3 \tag{54}$$

Nu_{Nai} is the Nusselt number associated with Sodium in the single-phase region given by W. M. Kays and M. E. Crawford[1;16].

$$h_{Nai} = \frac{Nu_{Nai}k_{Nai}}{Dh_{Nai}} \quad i = 1 \; or \; i = 3 \tag{55}$$

h_{Nai} is the convection heat transfer coefficient.

$$Uo_i = \frac{1}{\frac{1}{h_{Hei}} + \frac{1}{h_{Nai}}} \quad i = 1 \; or \; i = 3 \tag{56}$$

Disregarding the thermal resistance associated with the separation surface between the fluids, the global heat transfer coefficient in the single-phase region is represented by Uo_i.

$$h_{boil} = \mu_{Nal}h_{Nalv}\left(g\frac{(\rho_{Nal}-\rho_{Nav})^{0.5}}{\sigma_{Na}}\left(\frac{Cp_{Nal}}{Csfh_{Nalv}Pr_{Nal}}\right)^3\right)\Delta T_{sat}^2 \quad i = 2 \tag{57}$$

The boiling coefficient, h_{boil} in the two-phase flow region, Region 2, used in the simulation is associated with the nucleated boiling process. Equation (57) that presumably can be applied to processes related to liquid metals, according to Piyush Sabharwall *et al.,* [1], was determined experimentally by W. M. Rohsenow [17]. The Rohsenow equation is more uncomplicated such as that developed by J. C. Chen [18] and used by Piyush Sabharwall *et al.,* [1]. Equation (57) contains parameters that do not consider some complex effects, such as those occurring in convective boiling.

$$\Delta T_{sat} = T_{He2} - T_{Na2} \tag{58}$$

The saturation temperature difference is represented by ΔT_{sat}.

$$\sigma_{Na} == -0.1000989011d0 * TNa_2 + 204.8458973d0 \tag{59}$$

$\sigma_{Na}$is the surface tension associated with Sodium and can be found in a numerical table obtained by Joanne K. Fink and Leonard Leibowitz[14].

$$Csf = 0.006 \; fixed! \tag{60}$$

The parameter Csf is used in the work developed by W. M. Rohsenow[17].

$$Uo_i = \frac{1}{\frac{1}{h_{Hei}} + \frac{1}{h_{boil}}} \quad i = 2 \tag{61}$$

The global heat transfer coefficient represented by Uo_i, is associated with the boiling process occurring in Region 2.

$$A_{Tri} = \pi D_{hNai}L_i \quad 1 \leq i \leq 3 \tag{62}$$

The area of heat exchange between fluids is represented by A_{Tri}.

$$C_{Nal} = \dot{m}_{Na}Cp_{Nal} \quad Region \; 2 \tag{63}$$

$$C_{Nav} = \dot{m}_{Na}Cp_{Nav} \quad Region \; 2 \tag{64}$$

$$C_{Nai} = \dot{m}_{Na}Cp_{Nai} \quad i = 1 \; or \; i = 3 \tag{65}$$

$$C_{Hei} = \dot{m}_{He}Cp_{Hei} \quad 1 \leq i \leq 3 \tag{66}$$

$$C_i^* = \frac{C_i^{min}}{C_i^{max}} \quad 1 \leq i \leq 3 \tag{67}$$

The relationship between the fluids' minimum and maximum thermal capacities in region i is represented by C_i^*.

$$NTU_i = \frac{Uo_iA_{tri}}{C_i^{min}} \quad 1 \leq i \geq 3 \tag{68}$$

NTU_i is the number of thermal units in region i.

$$Fa_i = \frac{NTU_i(1-C_i^*)}{2} \quad 1 \leq i \leq 3 \tag{69}$$

Fa_i is the factor called "Fin Analogy Number" presented in the pioneering work of Fakheri A. [19] and used in papers developed by Élcio Nogueira [10-11].

$$\eta_{Ti} = \frac{Tanh(Fa_i)}{Fa_i} \quad 1 \leq i \leq 3 \tag{70}$$

η_{Ti} is the thermal efficiency in region i.

$$\varepsilon_{Ti} = \frac{1}{\frac{1}{\eta_{Ti}NTU_i} + \frac{1+C_i^*}{2}} \quad 1 \leq i \leq 3 \tag{71}$$

The thermal effectiveness in region i is represented by ε_{Ti}.

$$\dot{Q}_i = \varepsilon_{Ti} C_i^{min}(T_{Heini} - T_{Naini}) \; 1 \le i \le 3 \tag{72}$$

The heat transfer rate between the fluids in region i is obtained by $\dot{Q}_i$.

$$\dot{Q}_i^{Max} = C_i^{min}(T_{Heini} - T_{Naini}) \; 1 \le i \le 3 \tag{73}$$

$\dot{Q}_i^{Max}$ is the maximum heat transfer rate between the fluids in region i.

$$THe_{outi} = THe_{ini} - \frac{\dot{Q}_i}{C_i^{min}} \; 1 \le i \le 3 \tag{74}$$

THe_{outi} is the vapor helium outlet temperature in region i.

$$TNa_{outi} = TNa_{ini} + \frac{\dot{Q}_i}{C_i^{min}} \; i = 1 \; or \; i = 3 \tag{75}$$

The sodium outlet temperature is given by TNa_{outi}.

$$\sigma_{Ti} = \left(\frac{C_{Hei}}{C_i^{min}}\right) ln\left(\frac{THe_{outi}}{THe_{ini}}\right) + \left(\frac{C_{Nai}}{C_i^{min}}\right) ln\left(\frac{TNa_{outi}}{TNa_{ini}}\right) \; 1 \le i \le 3 \tag{76}$$

The thermal irreversibility in region i is represented by σ_{Ti}.

2.2 Hydraulic solution

$$f_{Hei} = [0.79Ln(Re_{Hei}) - 1.69]^{(-2)} \; 1 \le i \le 3 \tag{77}$$

$$\Delta P_{Hei} = \frac{4f_{Hei}\rho_{Hei}L_i V_{Hei}^2}{2Dh_{Hei}} \; 1 \le i \le 3 \tag{78}$$

$$f_{Nai} = [0.79Ln(Re_{Nai}) - 1.69]^{(-2)} \; 1 \le i \le 3 \tag{79}$$

$$\Delta P_{Nai} = \frac{4f_{Nai}\rho_{Nai}L_i V_{Nai}^2}{2Dh_{Nai}} \; 1 \le i \le 3 \tag{80}$$

f_{Hei} and f_{Nai} are the friction factors in region i. The pressure drops associated with helium and sodium fluids are represented through Equations (79) and (80).

$$P_{Heouti} = P_{Heini} + \Delta P_{Hei} \tag{81}$$
$$P_{Naouti} = P_{Naini} + \Delta P_{Nai} \tag{82}$$
$$R_i = \frac{T_{Heini} - T_{Heouti}}{T_{Naouti} - T_{Naini}} \; i = 1 \; or \; i = 3 \tag{83}$$
$$R_i = 1 \; i = 2 \; by \; definition \tag{84}$$
$$\sigma_{fi} = -\left(\frac{C_{Hei}}{C_i^{min}}\right) Rln\left(\frac{P_{Heini}}{P_{Heouti}}\right) - \left(\frac{C_{Nai}}{C_i^{min}}\right) Rln\left(\frac{P_{Naouti}}{P_{Naini}}\right) \; 1 \le i \le 3 \tag{85}$$

The viscous irreversibility in region i is represented by σ_{fi}.

$$\dot{S}_{geni} = C_i^{min}\sigma_{Ti} + C_i^{min}\sigma_{fi} \; 1 \le i \le 3 \tag{86}$$

$\dot{S}_{geni}$ is the entropy generation rate in region i.

$$Be_i = \frac{\sigma_{Ti}}{\sigma_{Ti} + \sigma_{fi}} \; 1 \le i \le 3 \tag{87}$$

The thermodynamic Bejan number is represented by Be_i.

3. RESULTS AND DISCUSSION

3.1 Region 1 - Sodium superheated steam

The simulations carried out in the region of superheated sodium vapor, called region 1, were implemented for two different situations about the diameter of the internal tube through which the sodium flows. The original diameter used by Piyush Sabharwal *et al.,* [1] is equal to 0.1220 m, and a second diameter used in the implementation of the model corresponds to a diameter equal to 0.2542 m. This last diameter value was used because it corresponds to the diameter associated with ¼ the speed of sound in region 2, where saturated sodium vapor flows.

The helium and sodium vapor inlet temperatures in region 1 equal 1027 ℃ and 883 ℃. Results were obtained for two different outlet temperatures for sodium, equal to 964 ℃ and 1000 ℃.
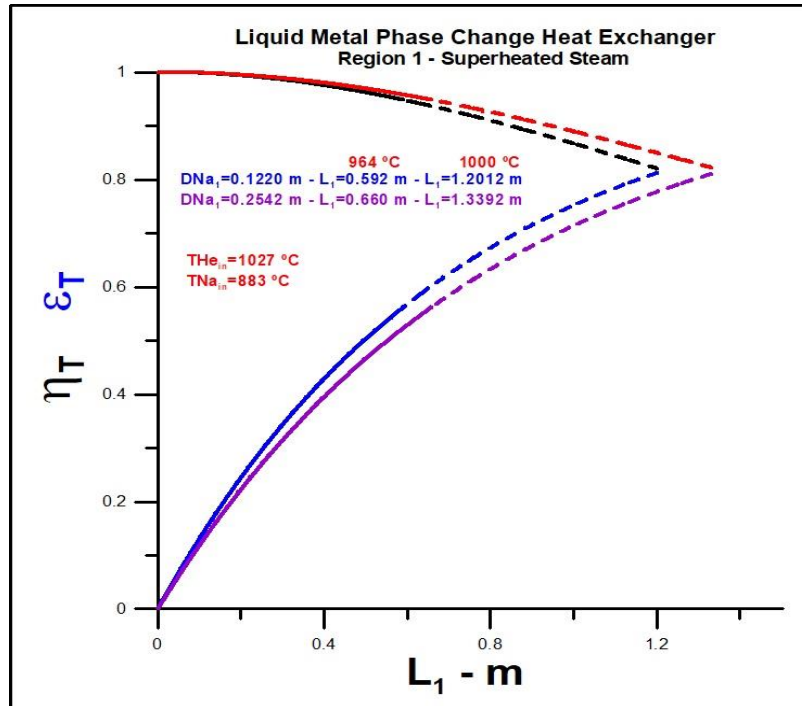
Figure 2: Thermal efficiency and thermal effectiveness for two different diameters in region 1 and two outlet temperatures
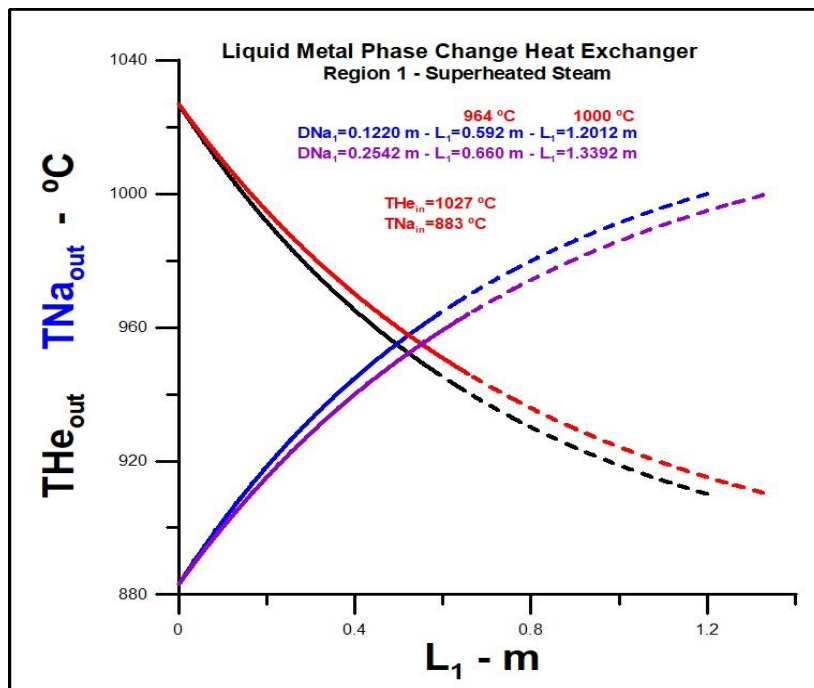
Figure 3: Outlet temperatures for helium and sodium for two different diameters in region 1 and two outlet temperatures

Results obtained for thermal efficiency and thermal effectiveness in region 1 are represented in Figure 2. The simulation used two different diameters for the internal diameter, diameter 0.1220 m, and diameter 0.2542 m. Thermal efficiency decreases with increasing pipe length, and thermal effectiveness increases with increasing pipe length. For a diameter equal to 0.1220 and sodium outlet temperature equal to 964 ℃, we have a pipe length in region 1 equal to 0.5908 meters, thermal efficiency equal to 0.9481, and thermal effectiveness equal to 0.5626 meters. When a higher outlet temperature

is required, equal to 1000 ℃, the length of the pipe in region 1 increases, to a value equal to 1.20 meters, the thermal efficiency decreases to 0.8205 and thermal effectiveness increases to 0.8125. Thermal performance improves when a higher value is imposed for the sodium vapor outlet temperature. When a higher value is set for the internal tube diameter, equal to 0.2542, the length of the pipe increases, and the thermal performance remains altered; that is, in terms of thermal performance, there is no reason to increase the diameter of the internal pipe in

region1 since greater piping length impacts the final costs of the heat exchanger.

The temperature profiles of the fluids in region 1 are represented in Figure 3, for two values of internal diameter. Consistent with the results presented in Figure 1, it can be seen that the outlet temperatures practically do not change with the increase in inner diameter. The helium vapor outlet temperature decreases with the increase in the sodium outlet temperature and the pipe's length. When the sodium outlet temperature equals 964 ℃, the helium vapor outlet temperature corresponds to 946 ℃, corresponding to approximately 911 ℃ for the sodium outlet temperature equals to 1000 ℃. The more demands are made on the heat exchanger, the greater the piping length required. When the internal diameter is increased from 0.1220 m to 0.2445 m, the length of the pipe rises to obtain the same helium vapor exit temperature values.
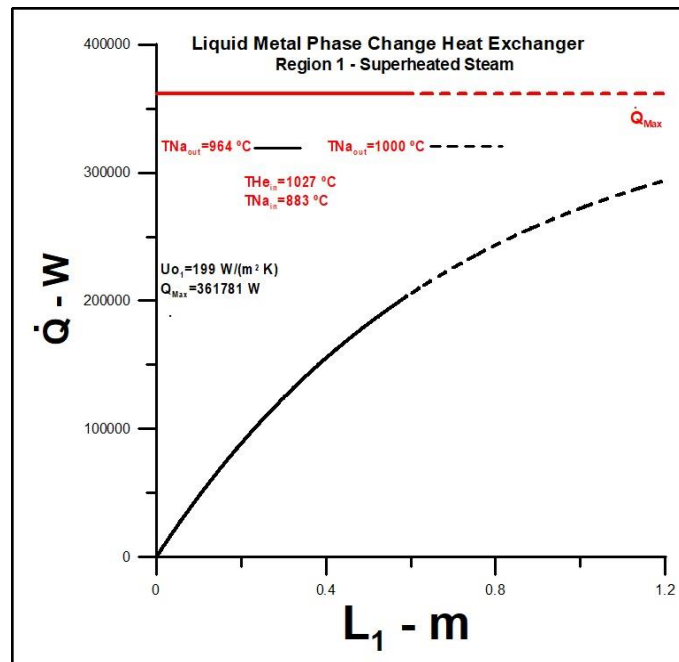
Figure 4: Heat transfer rate for internal diameter equal to 0.1220 m

The heat transfer rate is represented in Figure 4, for sodium internal diameter equal 0.1220 m. The heat transfer rate and the pipe length increase with the temperature required for the sodium vapor to exit. The thermal performance increases when the temperature of the outlet needed increases to 1000°C.
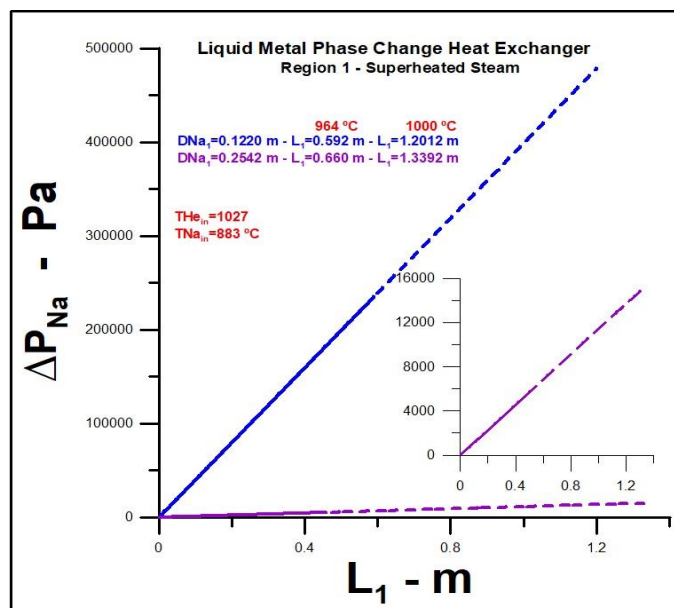
Figure 5: Pressure drop in the internal piping of region 1 for two internal diameter values and two outlet temperatures

As seen in Figure 5, the pressure drop associated with sodium increases with the increase in the outlet temperature required for sodium vapor, as well as with the length of the piping. However, when the pipe diameter is changed from 0.1220 m to 0.2542 m, there is a very significant decrease in the pressure drop due to the lower velocity in the pipe. The orders of magnitude of the values obtained are very different and are difficult to analyze on a single scale, and, in this sense, we present a highlighted figure for the pressure loss when the diameter is assumed to be equal to 0.2542 m. In terms of viscous dissipation, there is a great advantage in using an internal diameter equal to 0.2542 m.

The pressure drop that occurs in the annular region, where the helium vapor flow occurs, is represented in Figure 6 for two values of internal diameter. The pressure drop increases with tube length and with increases in the inner diameter. The increase in pressure drop for a larger internal diameter is justified by the smaller helium vapor flow area, which leads to a higher vapor velocity. However, a relevant fact is that the difference observed in the pressure drops is not as significant as in the internal pressure drop, marked in Figure 5. The values obtained in this case are of the same order of magnitude and very close.
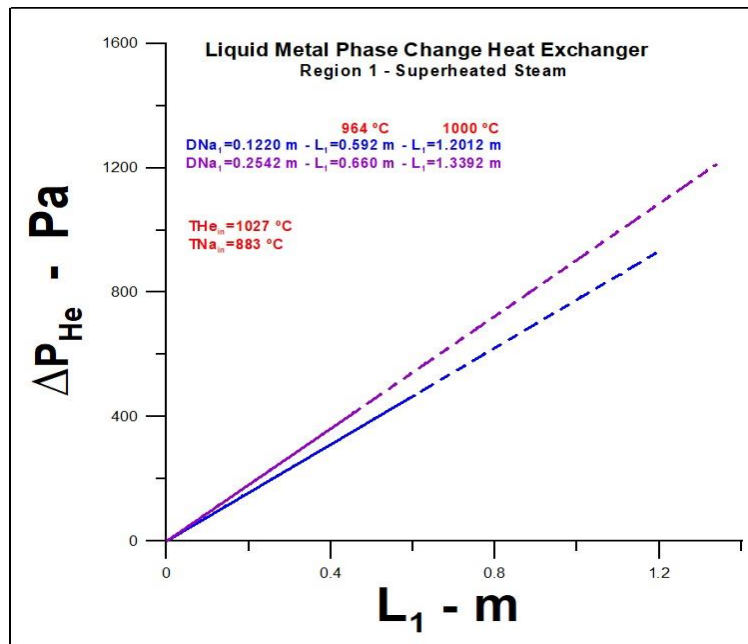
Figure 6: Pressure drop in the external piping of region 1 for two internal diameter values and two outlet temperatures
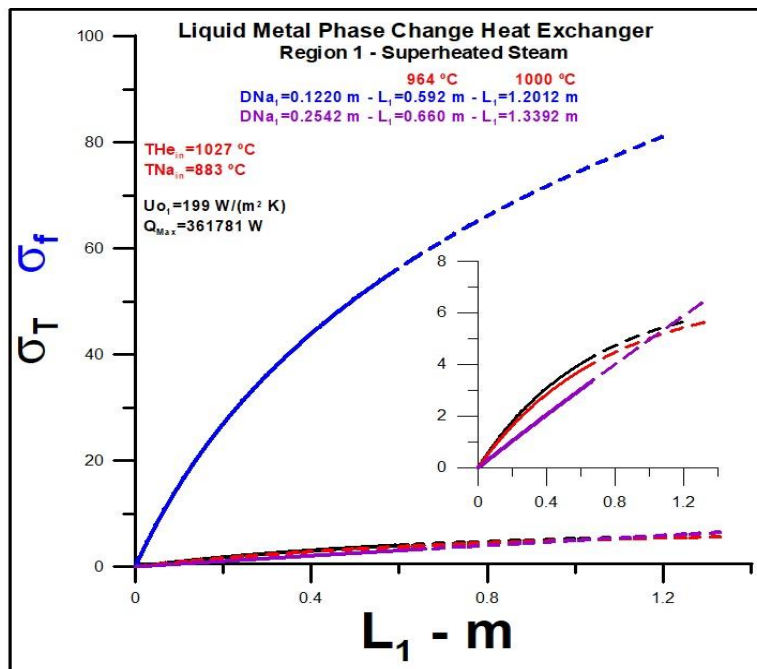
Figure 7: Thermal and viscous irreversibilities in region 1 for two internal diameter values and two outlet temperatures

Results for thermal and viscous irreversibilities in region 1 are represented in Figure 7 for two different internal diameters and two outlet temperatures for sodium. There is a significant difference, as expected based on the results presented in Figure 5, for viscous irreversibilities when comparing data related to internal diameter variation for sodium flow. In this case, the difference observed in irreversibilities is of an order of magnitude; that is, the viscous irreversibility related to sodium vapor for an internal diameter equal to 0.1220 m has a maximum value close to 80, and when related to an inner diameter equal to 0.2542 m it has a maximum value close to 7, as can be seen in the highlighted figure. The thermal irreversibilities, however, have values very close to each other, as shown in the highlighted figure, with results highlighted in black and red.
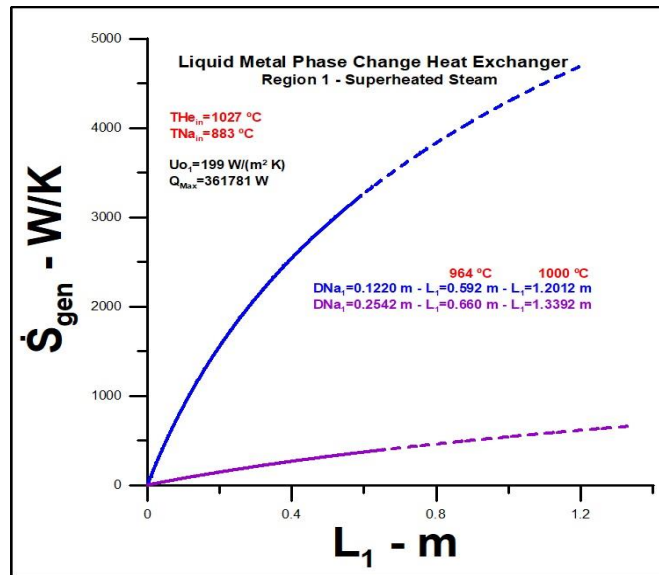
Figure 8: Entropy generation rate in region 1 for two internal diameter values and two outlet temperatures

As expected, the entropy generation rate in region 1, shown in Figure 8, presents very different results when the internal diameter varies from 0.1220 m to 0.2542 m. The entropy generation rate related to the inner diameter equal to 0.2542 m is 5 times lower than the entropy rate associated with the internal diameter equal to 0.1220 m. As previously discussed, this difference is mainly related to the velocity values associated with the inner duct.

The thermodynamic Bejan number in region 1 is represented in Figure 9. The result presented is highly promising regarding operational cost since higher values for the thermodynamic Bejan number are desired. Using an internal diameter in region 1 equal to 0.2542 m gives much better overall performance, and the cost-benefit ratio for the heat exchange is favorable.
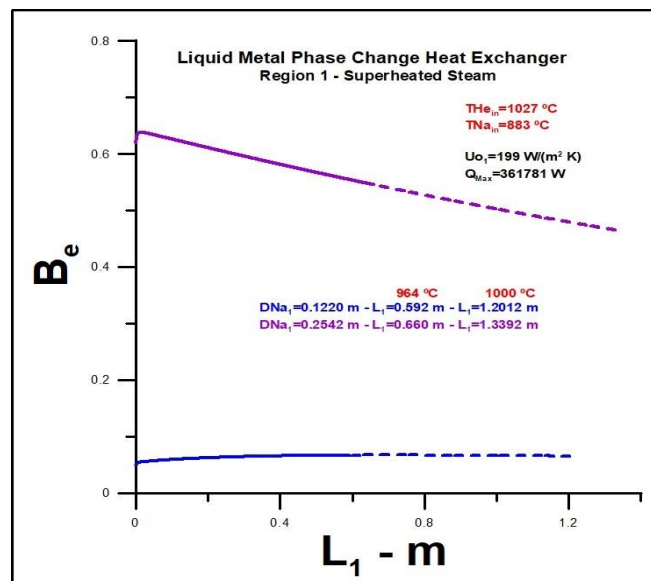
Figure 9: Bejan thermodynamic number in region 1 for two internal diameter values and two outlet temperatures

3.2 Region 2 - Sodium Saturated Steam

The exit temperature of the helium vapor in region 2 for two different internal diameters through which the sodium flows is shown in Figure 10. The diameters used in the simulation correspond to 0.1797 m and 0.2542 m. The minor diameter is associated with half the speed of sound in the internal duct, and the largest diameter corresponds to ¼ the speed. The helium exit temperature is imposed, equal to 900ºC, and the inlet equal 946 ºC. The length of the pipe necessary to reach the stipulated temperature is equal to 0.4 meters for the minor diameter, more significant than the length associated with the minor internal diameter, which corresponds to approximately 0.26 m. There is greater heat exchange for a larger diameter, related to a greater heat transfer area.

The thermal efficiency and effectiveness in region two are represented in Figure 11 for two different internal diameters. As expected, when thermal efficiency decreases, thermal effectiveness increases as the length of the pipe increases. The pipe size is more significant for the diameter corresponding to 1/2 the speed of sound in the internal duct when the helium vapor exit temperature is imposed equal to 900 ºC. The final lengths change for different diameters, but the absolute values for efficiency and effectiveness are the same for the two diameters analyzed. The effectiveness is relatively high, slightly greater than 0.8.
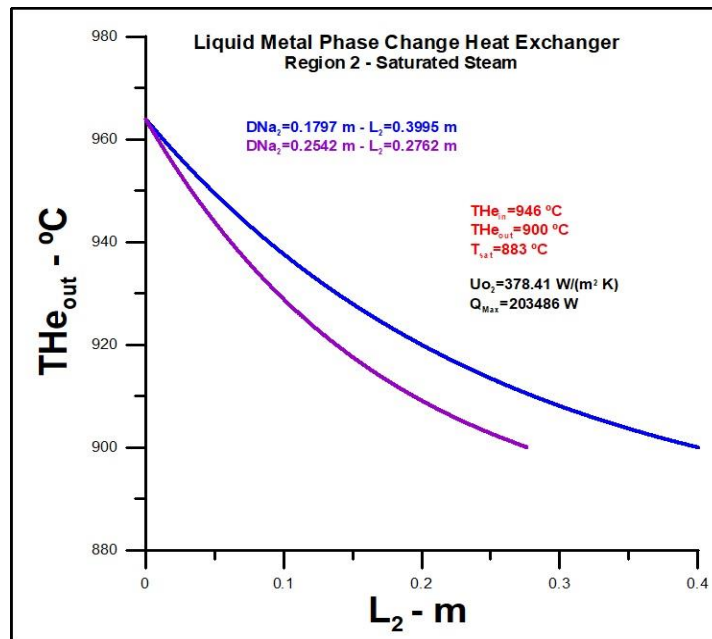
Figure 10: Outlet temperatures for helium for two different inner diameters in region 2
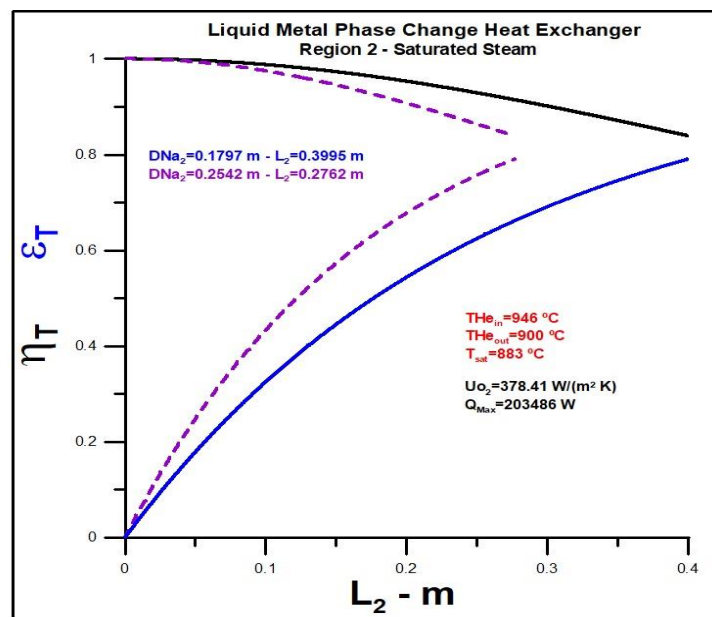
Figure 11: Thermal efficiency and thermal effectiveness for two different diameters in region 2
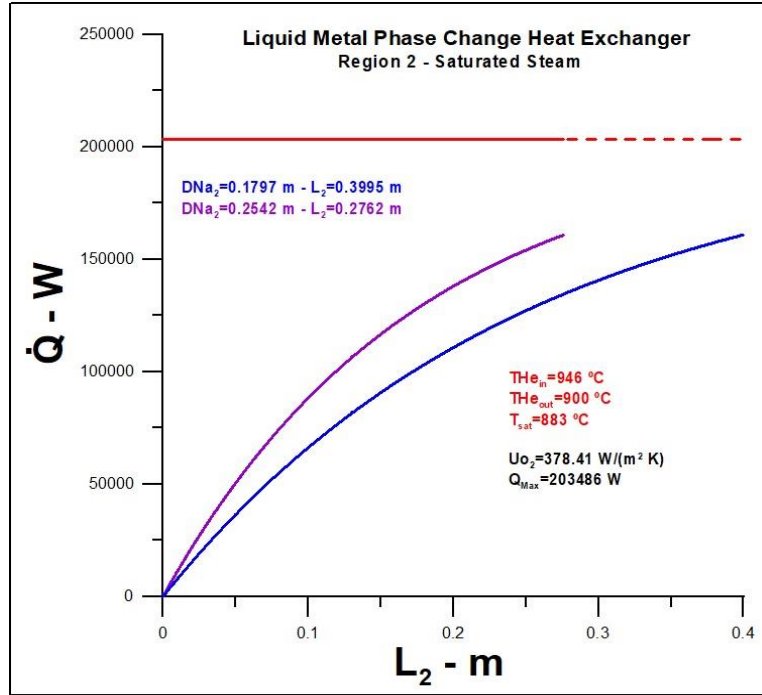
Figure 12: Heat transfer rate in the region 2 for two internal diameters
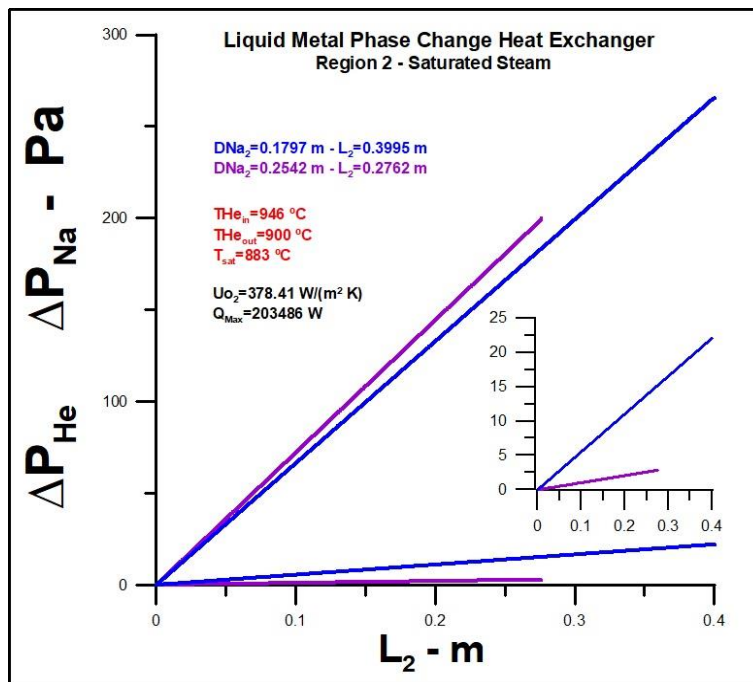
Figure 13: Pressure drops in the internal and the external piping of region 2 for two internal diameters

The heat transfer rate in region 2 is represented by Figure 12 for two internal diameters. The larger diameter's heat transfer rate is higher due to the larger heat transfer area. The maximum heat transfer rate is the same for both diameters because it depends on the inlet and outlet temperatures.

The pressure drops in region 2 associated with the internal and annular areas are represented in Figure 13. The pressure drop in the annular region, where the helium vapor flow occurs, is more significant than in the internal region, where sodium two-phase flow occurs. The difference in pressure drop observed between the two areas is of an order of magnitude. In the annular region, the greatest pressure drop is associated with the largest diameter due to the smaller passage area for helium vapor. On the other hand, in the internal region, the greatest pressure drop is related to the largest diameter.
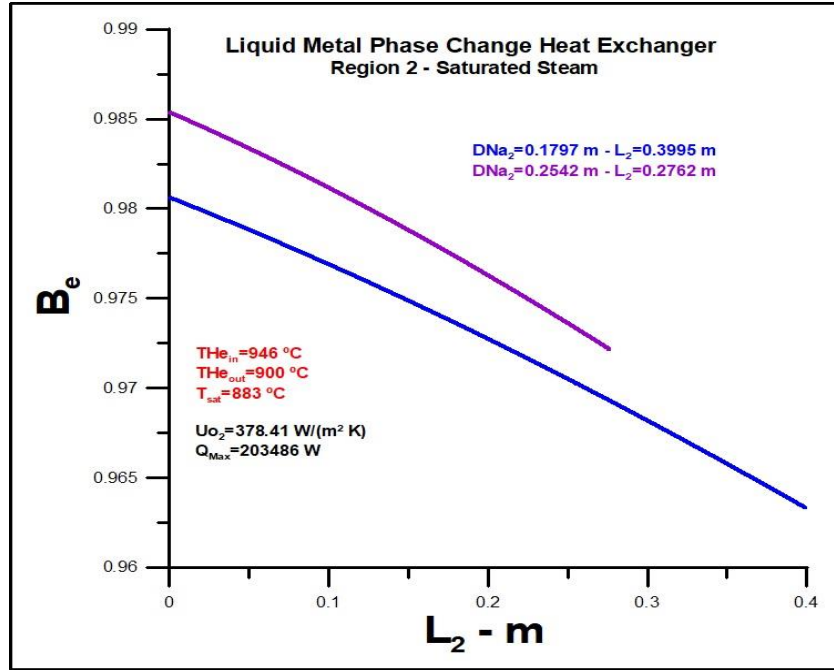
Figure 14: Bejan thermodynamic number in region 2 for two internal diameter values

The values obtained for the thermodynamic Bejan number in region 2 for the two diameters used in the simulation are very high, as shown in Figure 14. However, the absolute value for the larger diameter is slightly higher due to the greater exchange of heat.

3.3 Regions 3 – Sodium Subcooled Liquid

The temperature profiles for superheated helium vapor and subcooled sodium are represented in Figure 15. By imposition, the inlet temperatures equal 900 ºC and 120 ºC, and the sodium outlet temperature equals 833 ºC. The temperatures obtained for the helium vapor exit are the same for the two diameters analyzed, with a greater length of duct required for the smaller internal diameter due to less heat exchange. Thermal performance is significantly higher for the higher value diameter.
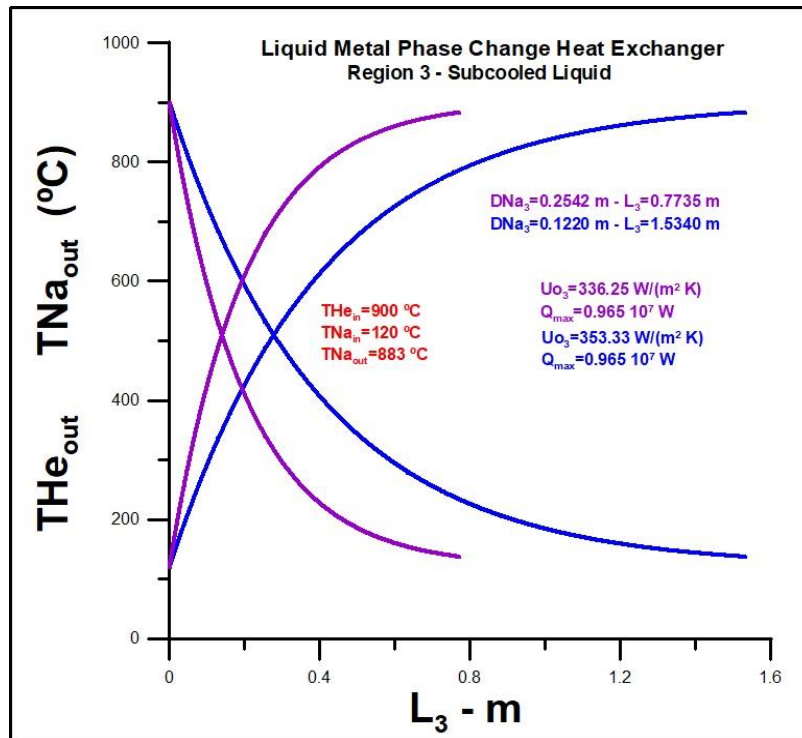
Figure 15: Outlet temperatures for helium and sodium for two different diameters in region 3
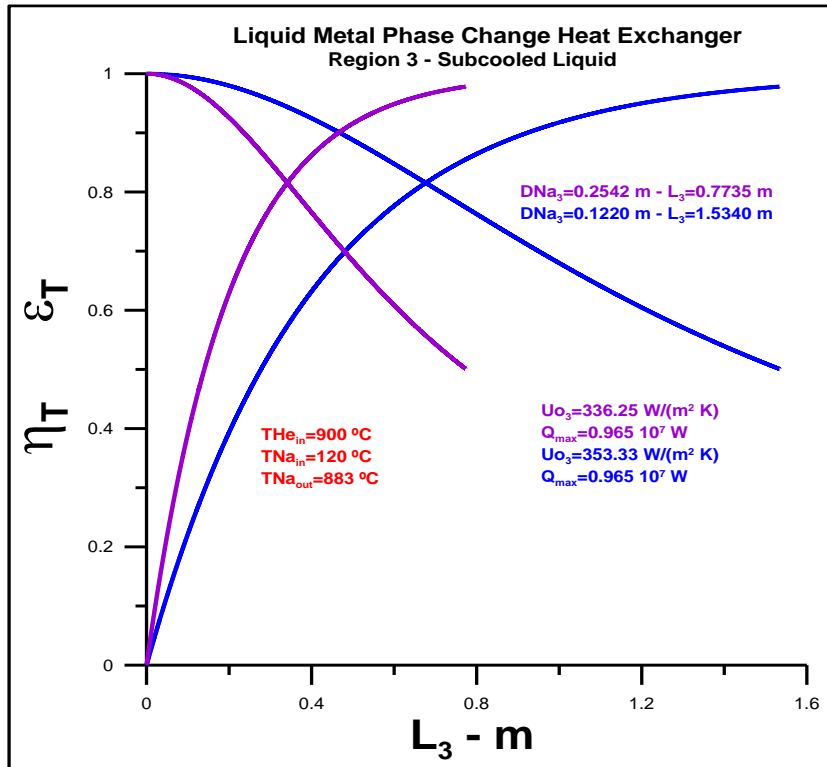
Figure 16: Outlet temperatures for helium and sodium for two different diameters in region 2

A Figura 16 apresenta resultados para eficiência térmica e efetividade térmica na região 3, para diâmetros iguais a 0.1220 m e 0.2542 m. As efetividades térmicas, para os dois diâmetros em análise, encontram-se muito próximas do valor máximo possível, entretanto o comprimento necessário para se alcançar as temperaturas estipuladas é significativamente menor para o maior diâmetro.
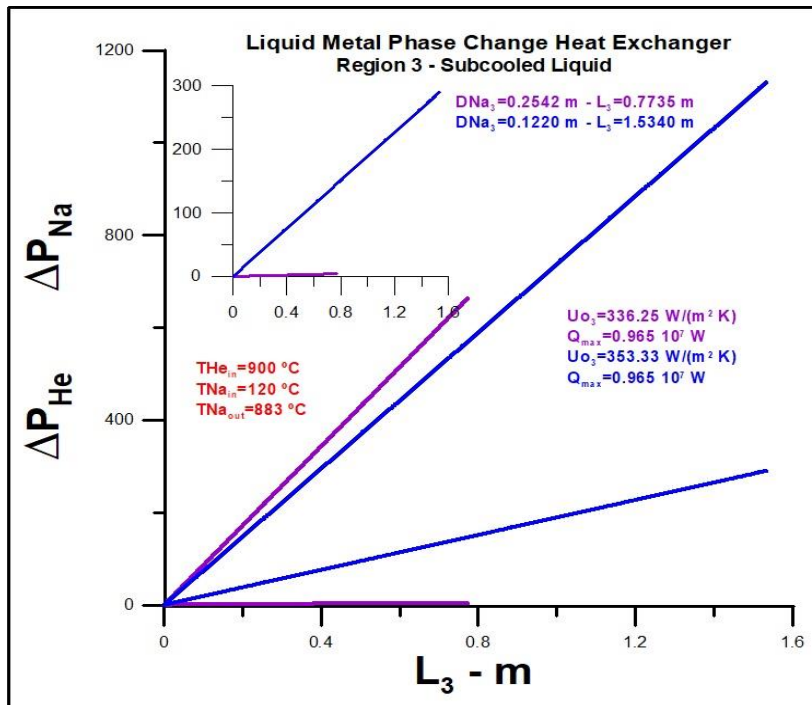
Figure 17: Pressure drops in the internal and the external piping of region 3 for two internal diameters

The pressure drops in the annular and internal regions are represented in Figure 17. The pressure drop in the annular region is significantly higher than in the inner region, where the flow of subcooled sodium occurs. The highlighted figure presents numerical values for the pressure drops associated with the two internal diameters

used in the simulation. It is observed that the pressure drop associated with a diameter equal to 0.2542 m is much smaller than the drop obtained for the pressure drop associated with a diameter equal to 0.1220 m, with indistinguishable values on the two scales used.

The relationship between thermal irreversibilities and total irreversibility, represented by the Bejan thermodynamic number, is shown in Figure 18. As already observed in Figure 16 and Figure 17, the operational performance relative to the 0.2542 m diameter is exceptional. Such exceptional operational performance in region 3 positively impacts the heat exchanger's final cost-benefit ratio.
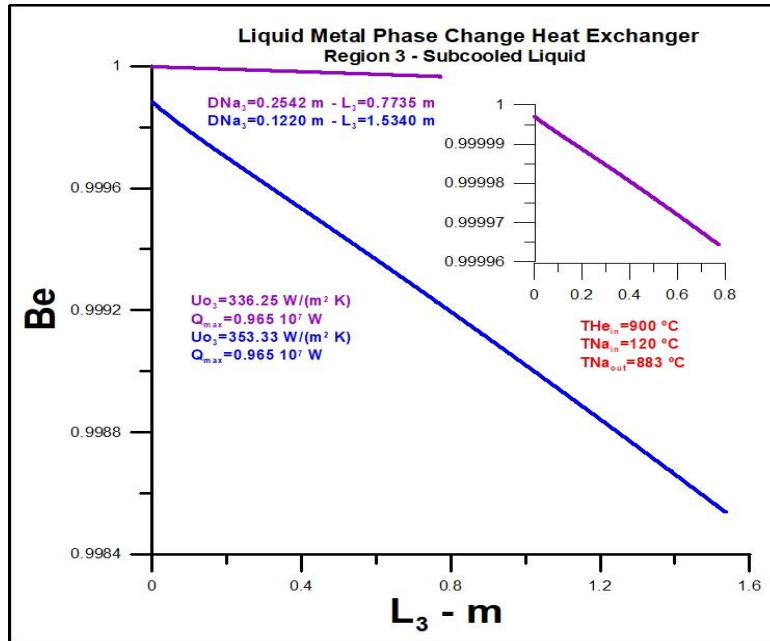
Figure 18: Bejan thermodynamic number in region 3 for two internal diameter values

3.4 Liquid Metal Phase Change Heat Exchanger – LMPCHE

This section will analyze the global performance of the heat exchanger, Liquid Metal Phase Change Heat Exchanger – LMPCHE, for different operating conditions associated with the internal diameters of the 3 regions under analysis. The inner diameter used in the simulations related to Figures 19 and 20 equals 0.2542 m. Table 1 presents performance results for MLPCHE in four different situations for comparison purposes.
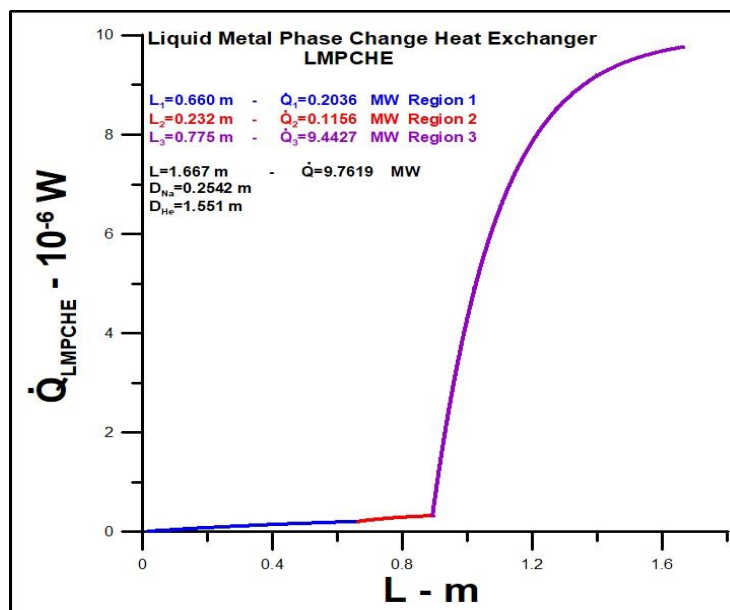
Figure 19: Heat transfer rate in LMPCHE
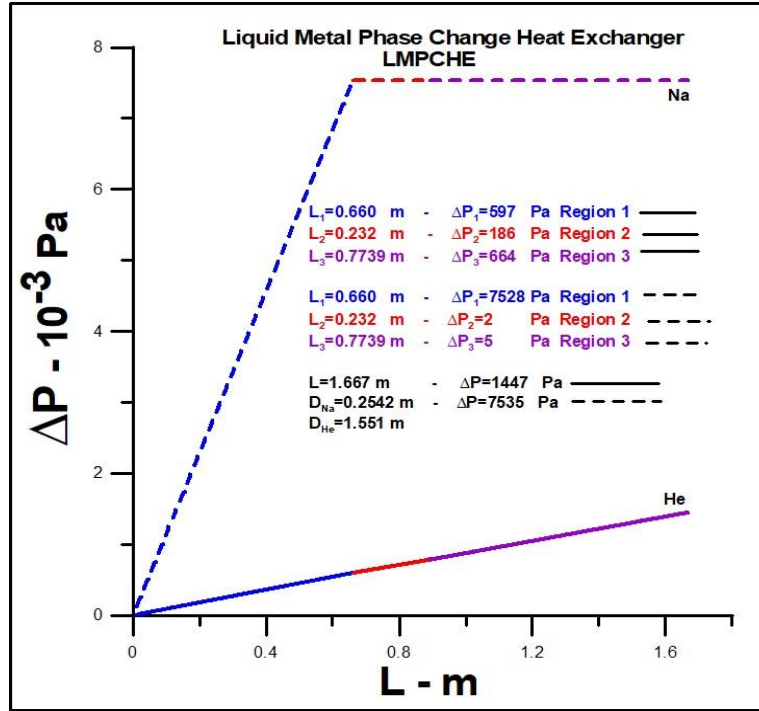
Figure 20: Pressure drop in LMPCHE

Table 1 below presents numerical simulation results for four configurations related to the LMPCHE heat exchanger under analysis. The first two configurations, with internal diameters equal to 0.1220 m, 0.1797 m, and 0.2542 m, were the subject of numerical analysis carried out by Piyush Sabharwall *et al.* [1] and serve as a basis for comparison with the two other simulations. The other two simulations are related to internal diameters equal to 0.1797 m or 0.2542 m in the three analyzed regions. The numerical results presented in the last column of the Table, related to inner diameters equal to 0.2542 m, surpass the other three simulations in terms of global performance. In this case, the pressure drops are significantly lower, the length of the piping associated with the LMPCHE heat exchanger presents a softer result, and, most importantly, the cost-benefit associated with the thermo-hydraulic performance, represented by the Bejan thermodynamic number, is very high.

Table 1: LMPCHE performance comparison for different operating conditions

D_{Na1}=0.1220 m D_{Na2}=0.1797 m D_{Na3}=0.1220 m	D_{Na1}=0.1220 m D_{Na2}=0.2542 m D_{Na3}=0.1220 m	D_{Na1}=0.1797 m D_{Na2}=0.1797 m D_{Na3}=0.1797 m	D_{Na1}=0.2542 m D_{Na2}=0.2542 m D_{Na3}=0.2542 m
$\Delta P_{He} = 1812\ Pa$	$\Delta P_{He} = 1757\ Pa$	$\Delta P_{He} = 1559\ Pa$	$\Delta P_{He} = 1447\ Pa$
$\Delta P_{Na} = 236566\ Pa$	$\Delta P_{Na} = 236550\ Pa$	$\Delta P_{Na} = 36419\ Pa$	$\Delta P_{Na} = 7535\ Pa$
σ_T=203.52	σ_T=203.52	σ_T=203.52	σ_T=203.52
σ_f=129.20	σ_f=129.20	σ_f=32.95	σ_f=7.71
Be=0.612	Be=0.612	Be=0.861	Be=0.964
L_{Total}=2.464 m	L_{Total}=2.360 m	L_{Total}=1.995 m	L_{Total}=1.667 m

Finally, to close the discussion on the simulation, some comparisons are made between quantities obtained through the model implemented by Piyush Sabharwall *et al.* [1] in Table 2.

Table 2: Some comparisons between models

Region 1	$U_0^{[1]} = 228.38$	$U_{o1} = 198.85$	Error=12.93%	W/(m² K)
Region 2	$U_0^{[1]} = 354.72$	$U_{o2} = 385.77$	Error=8.71%	W/(m² K)
Region 3	$U_0^{[1]} = 338.19$	$U_{o3} = 353.32$	Error=4.50%	W/(m² K)
Region 1	$h_{He}^{[1]} = 354.74$	$h_{He1} = 392.52$	Error=10.60%	W/(m² K)
Region 3	$h_{He}^{[1]} = 354.74$	$h_{He3} = 392.52$	Error=10.60%	W/(m² K)
Region 3	$Q_3^{[1]} = 1.03\ 10^7$	$Q_3 = 0.9443\ 10^7$	Error=8.30%	W

Relevant quantities for application and validation of the implemented model are found in Table 2. The quantities used for comparison are the global heat transfer coefficient in the three regions, the convective heat transfer coefficient in regions 1 and 3, and the heat transfer rate in region 3. The maximum percentage error obtained for the global coefficient is equal to 12.93%, the maximum percentage error obtained for the convective

heat transfer coefficient is equal to 10.60%, and he error for the heat transfer rate in region 3 is equal to 8.30%.

The theoretical model presented in this implementation is more straightforward and less complex than the model developed by Piyush Sabharwall *et al.* [1] used as a reference, mainly about region 2, where two-phase heat exchange occurs in Sodium. However, there are several discrepancies, and the current model can be improved if actual pipe lengths are used. Furthermore, using the nucleated boiling coefficient developed by W. M. Rohsenow [17] is only an pproximation for the two-phase convection phenomenon applied by Piyush Sabharwall *et al.* [1].

4 CONCLUSION

Theoretical analysis of heat exchange between Sodium in liquid metal and superheated helium vapor is carried out. Sodium enters the heat exchanger in the form of a subcooled liquid at a temperature equal to 120ºC, passes into saturated vapor at a temperature of 833ºC and leaves the heat exchanger as superheated vapor with a temperature in the range of 964ºC to 1000. The heat exchanger, called Liquid Metal Phase Change Heat Exchanger – LMPCHE, is part of a system that produces hydrogen coupled to a nuclear plant. The thermal and viscous irreversibilities in the three central regions of the heat exchanger are determined.

Four different configurations were simulated for comparison using sets of internal diameters related to sodium flow. It is demonstrated that when using inner diameters equal to 0.2542 m in the three regions under analysis, the overall performance of the heat exchanger, using Bejan's thermodynamic number, is exceptional, equal to 0.964. Furthermore, the length of the exchanger decreases to a value equal to 0.68 m, about the most extended length, equal to 2.464 m. In summary, the cost-benefit is very favorable when using a diameter in the three regions equal to 0.2542 m.

Numerical comparisons are made between the current model and the more elaborate and complex theoretical model obtained in the literature. Some parameters used in thecomparison are fundamental in determining the results presented, and the highest percentage error obtained corresponds to 12.93%. However, the current model does not adequately simulate some phenomena that occur in the heat exchange process, notably the two-phase heat exchange phenomenon, since the correlation used is valid for nucleated boiling, and the phenomenon observed is closer to convective boiling.

Although the correlation used in the model for two-phase heat exchange is more straightforward, has fewer empirical parameters, and allows a suitable resolution for the analyzed problem, it is expected that the use of a more complex correlation involving parameters related to essential phenomena that occur in

boiling convective, may be helpful to obtain more reliable theoretical results.

The main conclusions related to the simulation carried out are highlighted below:
1. The entropy generation rate in region 1 presents very different results when the internal diameter varies from 0.1220 m to 0.2542 m. The entropy generation rate related to the inner diameter equal to 0.2542 m is 5 times lower than the entropy rate associated with the internal diameter equal to 0.1220 m. The result is highly promising regarding operational cost since higher values for the thermodynamic Bejan number are desired. Using an internal diameter in region 1 equal to 0.2542 m gives much better overall performance, and the cost-benefit ratio for the heat exchange is favorable.
2. Values obtained for the thermodynamic Bejan number in region 2 for the two diameters used in the simulation are very high. However, the absolute value for the larger diameter is slightly higher due to the greater exchange of heat.
3. The relationship between thermal irreversibilities and total irreversibility, represented by the Bejan thermodynamic number, is exceptional. Such exceptional operational performance in region 3 positively impacts the heat exchanger's final cost-benefit ratio.
4. It was demonstrated that the overall performance of the heat exchanger under analysis is exceptional when the internal diameters are equal to 0.2542 m. The lower total length of the heat exchanger can offset the higher cost associated with using larger inner diameters.

5 NOMENCLATURE

Atr – heat transfer area, $[m^2]$

Cp – specific heat, $[\dfrac{J}{kg\,K}]$

C – thermal capacity, $[\dfrac{W}{K}]$

C_{min} – minimum thermal capacity, $[\dfrac{W}{K}]$

$C^* = \dfrac{C_{min}}{C_{max}}$

D_h – hydraulic diameter, $[m]$

Fa – fin analogy number

g – acceleration of gravity

h – coefficient of heat convection, $[\dfrac{W}{m^2 K}]$

He - Helium

k – thermal conductivity, $[\dfrac{W}{m\,K}]$

K - Kelvin

L – vertical or horizontal length, [m]

$\dot{m}$ – mass flow rate, [$\dfrac{kg}{s}$]

Na - sodium

Nu – Nusselt number

$\Pr$ – Prandtl number

$\dot{Q}$ – actual heat transfer rate, [W]

$\dot{Q}_{max}$ – maximum heat transfer rate, [W]

Re – Reynolds number

T – temperatures, [$^{\circ}C$]

Uo – global heat transfer coefficient, [$\dfrac{W}{m^2 K}$]

Subscripts
boil – boiling
i – region 1, 2 or 3
in – inlet
out – outlet
sat - saturation

Greek symbols

α – thermal diffusivity, [$\dfrac{m^2}{s}$]

ρ – density of the fluid, [$\dfrac{kg}{m^3}$]

μ – dynamic viscosity of the fluid, [$\dfrac{kg}{m\,s}$]

v – kinematic viscosity of the cold fluid, [$\dfrac{m^2}{s}$]

ε_T – thermal effectiveness

η_T – thermal efficiency

ΔT – a difference of temperatures, [ºC]

Acronyms: NTU – number of thermal units

REFERENCE

1. Piyush Sabharwall, Vivek Utgikar, Akira Tokuhiro & Fred Gunnerson (2009). "Design of Liquid Metal Phase Change Heat Exchanger for Next-Generation Nuclear Plant Process." Heat Application, Journal of Nuclear Science and Technology, 46:6, 534-544. DOI: 10.1080/18811248.2007.9711559

2. Piyush Sabharwall, Eung Soo Kim, and Nolan Anderson (2011). "Evaluation Metrics for Intermediate Heat Exchangers for Next Generation Nuclear Reactors." ANS 2011 Annual Meeting, Idaho National Laboratory, ID 83415-3860.

3. Piyush Sabharwall (2009). "Engineering Design Elements of a Two-Phase Thermosyphon to Transfer NGNP Thermal Energy to a Hydrogen Plant." Idaho National Laboratory Next Generation Nuclear Plant Project Idaho Falls, Idaho 83415. INL/EXT-09-15383 Revision 0.

4. Piyush Sabharwall, Fred Gunnerson, Akira Tokuhiro, Vivek Utgiker, Kevan Weaver, Steven Sherman (2007). "Theoretical Design of a Thermosyphon for Efficient Process Heat Removal From Next Generation Nuclear Plant (NGNP) for Production of Hydrogen." INL/EXT-07-13433. http://www.inl.gov

5. Anna M. Wagner (2014). "Review of Thermosyphon Applications." ERDC/CRREL TR-14-1. https://www.researchgate.net/publication/266672789

6. Bala Abdullahi, Raya K. Al-dadah, and Sa'ad Mahmoud (2019). "Thermosyphon Heat Pipe Technology". Recent Advances in Heat Pipes, IntechOpen. DOI: http://dx.doi.org/10.5772/intechopen.85410

7. Shanbin Shi, Yang Liu, Ilyas Yilgor, Piyush Sabharwall (2022). "A Two-Phase Three-Field Modeling Framework for Heat Pipe Application in Nuclear Reactors." INL /JOU-21-64836-Revision-0. http://www.inl.gov

8. Andrijana D. Stojanović, Srdjan V. Belošević, Nenad Dj. Crnomarković , Ivan D. Tomanović, AndAleksandar R. Milićević (2022). "NUCLEATE POOL BOILING HEAT TRANSFER Review of Models and Bubble Dynamics Parameters." THERMAL SCIENCE: Year 2022, Vol. 26, No. 1A, pp. 157-174. https://doi.org/10.2298/TSCI200111069S

9. Dawid Taler (2016). "Heat Transfer in Turbulent Tube Flow of Liquid Metals." Procedia Engineering 157 (2016) 148 – 157. doi: 10.1016/j.proeng.2016.08.350

10. Élcio Nogueira (2023). "A Theoretical Approach to be Applied in Heat Exchangers by Using the Thermal Efficiency Concept and the Second Law of Thermodynamic." Mechanical Engineering Advances 2023; 1(1): 92. http://dx.doi.org/10.59400/mea.v1i1.92

11. Nogueira, E. (2023). "Localized Theoretical Analysis of Thermal Performance of Individually Finned Heat Pipe Heat Exchanger for Air Conditioning with Freon R404A as Working Fluid." Journal of Materials Science and Chemical Engineering, 11, 61-85. https://doi.org/10.4236/msce.2023.118005

12. Petersen, H. (1970). "The Properties of Helium: Density, Specific Heats, Viscosity, and Thermal Conductivity at Pressures From 1 To 100 Bar and From Room Temperature to About 1800 K. "Risø National Laboratory. Denmark. Forskningscenter Risoe. Risoe-R No. 224.

13. Vincent D. Arp and Robert D. McCarty (1989). "Thermophysical Properties of Helium-4 From 0.8 to1500 K With Pressures to 2000 M Pa."

14. Joanne k. Fink and Leonard Leibowitz (1979). "Thermophysical Properties of Sodium." Chemical Engineering Division, Argonne Laboratory, ANL-CEN-RSD-79-1.15.

15. G. H. Golden and J. V. Tokar (1967). "Thermophysical Properties of Sodium." Argonne National Laboratory, ANL—7323 Chemistry (TID-4500), AEC Research and Development Report.

16. W. M. Kays, M. E. Crawford (1993). "Convective Heat and Mass Transfer." McGraw-Hill, Inc., New York.

17. W. M. Rohsenow (1952). "Heat transfer, a Symposium." Engineering Research Institute, University of Michigan, Ann Arbor, Michigan (1952).

18. J. C. Chen 91963). "A Proposed Mechanism and Method of Correlation for Convective Boiling Heat Transfer with Liquid Metals." Brookhaven National Laboratory, BNL 7319 (1963).

19. Fakheri A. (2007). "Heat Exchanger Efficiency." Journal of Heat and Mass Transfer; 129(9): 1268–1276. doi: 10.1115/1.2739620.